Acid−Base Equilibria of (2,2′-Bipyridyl-4,4′-dicarboxylic acid)ruthenium(II) Complexes and the Effect of Protonation on Charge-Transfer Sensitization of Nanocrystalline Titania

Md. K. Nazeeruddin,* S. M. Zakeeruddin, R. Humphry-Baker, M. Jirousek, P. Liska, N. Vlachopoulos, V. Shklover,† Christian-H. Fischer,‡ and M. Grätzel*

Laboratory for Photonics and Interfaces, Institute of Physical Chemistry, Swiss Federal Institute of Technology, CH-1015 Lausanne, Switzerland

Received August 2, 1999

The ruthenium complexes $[Ru(dcbpyH_2)_2(Cl)_2]$ (**1**), $[Ru(dcbpyH_2)_2(NCS)_2]$ (**2**), $(Bu_4N)_4[Ru(dcbpy)_2(NCS)_2]$ (**3**), and $(Bu_4N)_2[Ru(dcbpyH)_2(NCS)_2]$ (**4**) were synthesized and characterized by cyclic voltammetry, UV−vis absorption, and emission, IR, Raman, and NMR spectroscopy. The absorption and emission maxima of these complexes red shifted with decreasing pH, and showed pH-dependent excited-state lifetimes. The ground-state pK_a values were determined by spectrophotometeric methods, and the dissociation of protons was found to occur in two steps (pK_a = 3 and 1.5). The Ru(II)/(III) couple in the complex $(Bu_4N)_4[Ru(dcbpy)_2(NCS)_2]$ is shifted ca. 290 mV negatively with regard to that of the complex $[Ru(dcbpyH_2)_2(NCS)_2]$ due to the replacement of H^+ by tetrabutylammonium cation. The negative shift for the dcbpy-based reduction potential is even larger, i.e., about 600 mV compared to that of the complex $[Ru(dcbpyH_2)_2(NCS)_2]$. The effect of deprotonation on the performance of these complexes as photosensitizers for nanocrystalline titania was investigated.

Introduction

The sensitization of nanocrystalline titania by ruthenium(II) complexes containing a 2,2′-bipyridyl-4,4′-dicarboxylic acid ligand is presently under intense investigation in many laboratories.[1−3] Dye-derivatized mesoporous titania films are the key component of a new solar cell for which certified solar to electric power conversion efficiencies between 10% and 11% have been obtained.[4] Moreover, when ruthenium complexes are employed as sensitizers, these cells show excellent stability, making practical applications feasible.[5]

To obtain high conversion efficiencies, optimization of the short-circuit photocurrent i_{sc} and open-circuit potential V_{oc} of the solar cell is essential. The conduction band of the TiO_2 is known to have a Nernstian dependence on pH.[1a,6] The fully protonated sensitizer upon adsorption transfers most of its protons to the TiO_2 surface, charging it positively. The electric field associated with the surface dipole generated in this fashion enhances the adsorption of the anionic ruthenium complex and assists electron injection from the excited state of the sensitizer to the titania conduction band, favoring high photocurrents.[7] However, the open-circuit potential will be low due to the positive shift of the conduction band edge induced by surface protonation. On the other hand, if the sensitizer carries no protons at all, one expects a high value for V_{oc} while that for i_{sc} will be low. Thus, there should be an optimal degree of protonation of the sensitizer for which the product of the short-circuit photocurrent and open-circuit potential which determines the power conversion efficiency of the cell reaches a maximum. Deprotonation of the ruthenium complex also increases its solubility. Higher concentrations are desirable as they accelerate the dye uptake onto the TiO_2 surface and facilitate its purification by recrystallization from organic solvents.[8]

In the present paper we report the synthesis and characterization of bis(4,4′-dicarboxy-2,2′-bipyridine)ruthenium(II) complexes with different degrees of protonation and a systematic study of their absorption, emission, electrochemical, and photoelectrochemical properties.

Experimental Section

Materials. The solvents (puriss grade) tetrabutylammonium hydroxide and potassium thiocyanate (KNCS) were obtained from Fluka.

† Laboratory of Crystallography, Swiss Federal Institute of Technology, 8092 Zurich, Switzerland.

‡ Hahn-Meitner-Institut Berlin, D-14109 Berlin, Germany.

(1) Huang, S. Y.; Schlichthörl, G.; Nozik, A. J.; Grätzel, M.; Frank, A. J. *J. Phys. Chem. B* **1997**, *101*, 2576. (b) Schlichthörl, G.; Huang, S. Y.; Sprague, J.; Frank, A. J. *J. Phys. Chem. B* **1997**, *101*, 8142. (c) Papageorgiou, P.; Barbé, C.; Grätzel, M. *J. Phys. Chem. B* **1998**, *102*, 4156. (d) Nazeeruddin, Md. K.; Grätzel, M. GB Patent 9217811, **1994**. (e) Dloczik, L.; Ileperuma, O.; Lauermann, I.; Peter, L. M.; Ponomarev, E. A.; Redmond, G.; Shaw, N. J.; Uhlendorf, I. *J. Phys. Chem. B* **1997**, *101*, 10281. (f) Sughihara, H.; Sing, L. P.; Sayama, K.; Arakawa, H.; Nazeeruddin, Md. K.; Grätzel, M. *Chem. Lett.* **1998**, 1005. (g) Sayama, K.; Sughihara, H.; Arakawa, H. *Chem. Mater*. **1998**, *10*, 3825. (h) Salafsky, J. S.; Lubberhuizen, W. H.; van Faassen, E.; Schropp, R. E. I. *J. Phys. Chem. B* **1998**, *102*, 766.

(2) (a)Murakoshi, K.; Kano, G.; Wada, Y.; Yanagida, S.; Miyazaki, H.; Matsumoto. M.; Murasawa, S. *J. Electroanal. Chem*. **1995**, *396*, 27. (b) Nasr, C.; Hotchandani, S.; Kamat, P. V. *J. Phys. Chem. B* **1998**, *102*, 4944−4951. (c) Das, S.; Kamat, P. V. *J. Phys. Chem. B* **1998**, *102*, 8954−8957. (d) Ihara, M.; Tanaka, K.; Sakaki, K.; Honma, I.; Yamada, K. *J. Phys. Chem. B* **1997**, *101*, 5153.

(3) Alebbi, M.; Bignozzi, C. A.; Heimer, T. A.; Hasselmann, G. M.; Meyer, G. J. *J. Phys. Chem. B.* **1998**, *102*, 7577. (b) Argazzi, R.; Bignozzi, C. A.; Heimer, T. A.; Meyer, G. J. *Inorg. Chem*. **1997**, *36*, 2. (c) Argazzi, R.; Bignozzi, C. A.; Hasselmann, G. M.; Meyer, G. J. *Inorg. Chem*. **1998**, *37*, 4533. (d) Zaban, A.; Ferrrere, S.; Sprague, J.; Gregg, B. A. *J. Phys. Chem. B* **1997**, *101*, 55.

(4) Nazeeruddin, Md. K.; Kay, A.; Rodicio, I.; Humphry-Baker, R.; Muller, E.; Liska, P.; Vlachopoulos, N.; Grätzel, M. *J. Am. Chem. Soc*. **1993**, *115*, 6382.

(5) Kohle, O.; Grätzel, M.; Meyer, A. F.; Meyer, T. B. *Adv. Mater*. **1997**, *11*, 904.

(6) Nozik, A. J. *Annu. Rev. Phys. Chem*. **1978**, *29*, 189. (b) Yan, S.; Hupp, J. T. *J. Phys. Chem*. **1996**, *100*, 6867. (c) Watanabe, T.; Fujishima, A.; Tatsuoki, O.; Honda, K. *Bull. Chem. Soc. Jpn*. **1976**, *49*, 8. (d) Gerisher, H. *Electrochim. Acta* **1989**, *34*, 1005.

(7) Pelet, S.; Moser, J. E.; Grätzel, M. Submitted to *J. Phys. Chem. B.*

(8) Kohle, O.; Ruile, S.; Grätzel, M. *Inorg. Chem*. **1996**, *35*, 4779.

10.1021/ic990916a CCC: $18.00
Published on Web 12/09/1999

Hydrated ruthenium trichloride was purchased from Johnson-Mathey and used as received. 4,4′-Dicarboxy-2,2′-bipyridine (dcbpy)[9] was synthesized using the literature procedure.

Analytical Measurements. UV−vis and fluorescence spectra were recorded in a 1 cm path length quartz cell on a Cary 5 spectrophotometer and Spex Fluorolog 112 spectrofluorometer, respectively. The measured emission and excitation spectra were routinely corrected for the wavelength-dependent features. The solutions were prepared in ethanol to give approximate concentrations of 10 μM, and purged with nitrogen in the cases where emission quantum yields were reported. The emission lifetimes were measured in an air-saturated ethanol solution by exciting the sample with a pulse from an active mode-locked Nd:YAG laser, using the frequency-doubled line at 532 nm. The emission decay was followed on a Tektronix DSA 7912 digitizing signal analyzer, having used a Hamamatsu R928 photomultiplier to convert the light signal to a voltage signal.

Electrochemical data were obtained by cyclic voltammetry using a conventional single-compartment three-electrode cell and a PAR potentiostat model 273. The working electrode was a 25 μm Pt microdisk, the auxiliary electrode was a platinum wire, the reference electrode was a silver wire, and the supporting electrolyte was 0.1 M TBATFB (tetrabutylammonium tetrafluoroborate). Proton and ^{13}C NMR spectra were measured on a Bruker 200 MHz spectrometer. The reported chemical shifts were against TMS. Infrared spectra were obtained with a Perkin-Elmer Paragon 1000 FTIR spectrophotometer at a resolution of 5 cm^{-1} with the samples dispersed in compressed KBr pellets.

Resonance Raman spectra were obtained on a 1877 Triplemate spectrograph equipped with a Princeton Instruments liquid N_2 cooled CCD-1024E detector. A 1200 groove/mm grating was used, giving a resolution of 2.5 cm^{-1}. Data acquisition was controlled by an Apple Power PC computer running Wavemetrics software to control the PI ST-135 controller and the Spex DM 3000 controller. All the data were corrected for the spectral response of the instrument using a National Bureau of Standards light standard. An INNOVA 200K Kr^+ laser provided the excitation source.

X-ray Structure Determination. Single crystals of the [Ru(dcbpyH$_2$)$_2$(NCS)$_2$] complex were obtained from DMSO solvent. When the solvent was allowed to evaporate slowly, the complex [Ru(dcbpyH$_2$)$_2$(NCS)$_2$] deposited as small crystals onto the walls of the flask. The data collection for a single crystal was performed at 243 K on a Siemens with a CCD detector, using a Mo Kα radiation source with a graphite monochromator. An ω-scan technique with an exposure time of 120 s/frame for each image was used. Experimental details and results of the structure refinement are depicted in Table 4. The H atoms were not localized, but in bipyridyl moieties they were placed in calculated positions and refined as "riding" atoms with fixed C−H distances and isotropic temperature factors $U = 0.08$ Å^2. The O and C atoms of solvate DMSO molecules were refined isotropically. SHELXTL PLUS[10] software was used for data reduction, structure solution, and refinement. A full description of the single-crystal study of **2** is given in our previous paper.[11]

High-Performance Liquid Chromatography (HPLC). HPLC analysis was carried out using a Waters 991 multichromatogram. The stationary phase is a fine solid material, typically 5−10 μm in diameter. The sample solution was introduced into the liquid stream by a sample loop immediately before the column. The eluent was pumped with a constant flow rate through the separation column. The separated components from the column were detected by a diode array spectrophotometer, which allows for the rapid measurement of the complete UV−vis absorption spectra. The result is a three-dimensional data set consisting of retention time, wavelength, and extinction.

Synthesis. Synthesis of *cis*-Dichlorobis(2,2′-bipyridyl-4,4′-dicarboxylic acid)ruthenium(II), 1. This complex was synthesized using a slight modification of our previous procedure.[4] $RuCl_3(H_2O)_3$ (0.523 g, 2 mmol) was dissolved in 50 mL of DMF under argon. After the solution was stirred for 15 min, another 50 mL of DMF was added. To this solution was added 2,2-bipyridine-4,4′-dicarboxylic acid ligand as a solid (0.952 g, 3.9 mmol). The flask was immersed in an oil bath that was maintained at 170−180 °C while the contents were refluxed with vigorous stirring for 3 h under the dark and an argon atmosphere. The progress of the reaction was monitored by UV−vis spectra. At the end of the reaction, the relative intensities of the absorption maxima in ethanol at 565, 414, and 316 nm were 1:1.05:3.33. The reaction mixture was allowed to cool to room temperature and filtered through a sintered glass crucible. The solvent DMF was evaporated completely on a rotary evaporator under vacuum. The resulting solid product was washed with a 1:4 mixture of acetone and diethyl ether. The solid was stirred again in 100 mL of 2 M HCl for 4 h in darkness, and the mixture was filtered through a sintered glass crucible. After drying, the yield was 1.14 g (87%). Anal. for [RuL$_2$(Cl)$_2$], C24, H16, N4, O8, Cl2, Ru. Calcd (%): C, 43.67; H, 2.44; N, 8.48; Cl, 10.74. Found: C, 44.02, H, 2.48, N, 8.90; Cl, 10.74.

Synthesis of *cis*-Dithiocyanatobis(2,2′-bipyridyl-4,4′-dicarboxylic acid)ruthenium(II), 2. A 5.82 g (60 mmol) sample of KNCS was dissolved in 10 mL of distilled water and transferred into a three-necked flask. To this solution was added 50 mL of DMF, which was then purged with Ar for 15 min. A 1.1 g (1.7 mmol) sample of [RuL$_2$(Cl)$_2$] was introduced into the flask in darkness, followed by another 50 mL of DMF solvent. The flask was covered with an aluminum foil and refluxed for 5 h. The reaction mixture was allowed to cool and then filtered through a sintered glass crucible. The DMF and water solvents were removed using a rotary evaporator under high vacuum. To the resulting viscous liquid was added 20 mL of 0.2 M NaOH to give a dark purple-red homogeneous solution. The solution was filtered, and the pH was lowered to 3.5 with an acid solution of 0.5 M HNO_3 or CF_3SO_3H to give a dense precipitate. The flask was placed in a refrigerator for 12 h. After the flask was warmed to room temperature, the solid was collected on a sintered glass crucible by suction filtration. The solid was washed (3 × 20 mL) with pH 3.5 water that was acidified with the same acid as previously used and air-dried. Yield 0.9 g, 85%. Anal. for [RuL$_2$(NCS)$_2$]·4(H$_2$O), C26, H24, N6, O12, S2, Ru. Calcd (%): C, 40.15; H, 3.11; N, 10.80; S, 8.24. Found: C, 39.65; H, 3.13; N, 10.53; S, 8.67.

Synthesis of Tetrakis(tetrabutylammonium) *cis*-Dithiocyanatobis(2,2′-bipyridine-4,4′-(COO$^-$)$_2$)ruthenium(II), 3. A 0.5 g sample of the complex **2** was introduced into a 250 mL conical flask containing 50 mL of distilled water. To this solution was added dropwise 10% tetrabutylammonium hydroxide solution till the pH of the solution showed a stable reading of pH 7. At this stage, the solution was filtered through a sintered glass crucible, and the solvent was removed on a rotary evaporator. The resulting viscous liquid was dissolved in methanol and precipitated by the addition of 1:1 diethyl ether and petroleum ether mixture. The solid that was precipitated as a hygroscopic substance was dried under vacuum for 24 h. Anal. for (TBA)$_4$[RuL$_2$(NCS)$_2$]·4(H$_2$O), C90, H162, N10, O12, S2, Ru. Calcd.: C, 62.07; H, 9.38; N, 8.04. Found: C, 61.85; H, 9.03; N, 7.93.

Synthesis of Bis(tetrabutylammonium) *cis*-Dithiocyanatobis(2,2′-bipyridine-4-COOH,4′-COO$^-$)ruthenium(II), 4. Complex **4** is a nonhygroscopic air-stable solid, which is the doubly protonated species of complex **3**. It was obtained by titrating complex **3** with a 0.1 M nitric acid solution. In a typical synthesis, 1 g of complex **3** was weighed into a 100 mL round-bottom flask and dissolved in 10 mL of distilled water. The pH of this solution was lowered to 3.8 by the addition of 0.1 M nitric acid. At this pH most of the complex precipitates out and the flask was kept in a refrigerator for 12 h. The flask was allowed to warm to room temperature (25 °C), and the precipitate was collected on a sintered glass crucible. The isolated solid was washed once with 5 mL of pH 3.8 water. The dried product was 0.6 g, yield 80%. Anal. for (TBA)$_2$(H)$_2$ [RuL$_2$(NCS)$_2$]·4(H$_2$O), C58, H92, N8, O12, S2, Ru. Calcd: C, 53.5; H, 7.5; N 8.61. Found: C, 53.65; H, 7.47; N, 8.93.

Results and Discussion

1. Absorption Spectra. The complex *cis*-[Ru(dcbpyH$_2$)$_2$(Cl)$_2$] is soluble in organic solvents and undergoes cis-to-trans

(9) Nazeeruddin, Md.; Kalyanasundaram, K.; Grätzel, M. *Inorg. Synth*. **1997**, *32*, 181.
(10) Sheldrick, G. M. SHELXTL PLUS. VAX/VMS Version, Siemens Analytical X-ray Instruments Inc., Madison, WI, 1990.
(11) Shklover, V.; Ovchinnikov, Yu. E.; Braginsky, L. S.; Zakeeruddin, C.; Kay, A.; Grätzel, M. *Chem. Mater*. **1998**, 2533.

Table 1. Electronic Spectral Data of Complexes **1**−**4** in Ethanol[a]

complex	absorption λ(max) (nm) (ϵ/10^4 M^{-1} cm^{-1})			emission λ(max) (nm)[c]	τ (ns)[c]
$[Ru(dcbpyH_2)_2(Cl)_2]$	565 (1.1)	414 (1.0)	316 (3.45)	850	
$[Ru(dcbpyH_2)_2(NCS)_2]$	538 (1.42)	398 (1.40)	314 (4.82)	830	20
$(Bu_4N)_4[Ru(dcbpy)_2(NCS)_2]$[b]	518 (1.3)	380 (1.33)	308 (4.59)	750	60
$(Bu_4N)_2[Ru(dcbpyH)_2(NCS)_2]$	535 (1.47)	395 (1.43)	312 (4.91)	830	40

[a] The emission spectra were obtained by excitation at λ(max) of the complexes. [b] This complex is a hygroscopic solid, and the values in parentheses are ±10%. [c] Measured in an air-saturated ethanol solution at 298 K.

Table 2. Absorption and Emission Spectral Properties of Complex **3** in Different Organic Solvents at Room Temperature[a]

solvent	absorption max (nm)	emission max (nm)	dielectric constant (ϵ)
H_2O	500	720	100
CH_3CN	510	730	37.5
C_2H_5OH	518	750	24.55
C_2H_5CN	530	775	27.2
C_3H_7CN	540	800	20.3
1:1 C_3H_7CN/C_2H_5CN	536	790	20.3/27.2
DMSO	540	890	46.68

[a] The emission spectrum of complex **3** was obtained by excitation at λ 510 nm.

isomerization under light.[12] The chloride ligands in the *cis*-$[Ru(dcbpyH_2)_2(Cl)_2]$ complex are labile and in coordinating solvents such as water and DMSO are readily substituted to form the diaqua and DMSO complexes, respectively. The absorption spectral data of complexes **1**−**4**, in the UV−vis region, are presented in Table 1, and for convenience, the cis prefix notation will be omitted in further discussion. The absorption spectrum of the $[Ru(dcbpyH_2)_2(Cl)_2]$ complex in dry ethanol shows two broad visible bands at 560 and 410 nm that are assigned to metal-to-ligand charge-transfer (MLCT) origin.[13] The bands in the UV at 314 nm with a shoulder at 304 nm are assigned as intraligand ($\pi-\pi^*$) charge-transfer transitions.[13] Similarly, complex **2**, in ethanol, shows two intense visible bands at 538 and 398 nm. The longer wavelength band of complex **2** is 25 nm red shifted when compared to that of the analogous unsubstituted bpy.[14] This red shift is mainly due to the electron-withdrawing nature of the COOH groups at the 4,4′-positions of the bipyridine ligand, which lowers the energy of the π^* orbital of the ligand.[15]

Deprotonation of the COOH groups in complex **2** blue shifts the $\pi-\pi^*$ charge-transfer band from 314 to 308 nm, and the low-energy MLCT band shifted to higher energy by 20 nm, from 538 to 518 nm. The blue shift is due to an increase in the energy of the LUMO of the ligand, causing the $\pi-\pi^*$ and $d\pi-\pi^*$ transitions to occur at higher energies.[16]

The absorption spectral properties of complex **3** as a function of solvent polarity are gathered in Table 2. For complex **3**, the most intense lowest energy MLCT feature varies from 500 nm (in H_2O) to 510 nm (in CH_3CN) to 540 nm (in C_3H_7CN). The observed 40 nm blue shift in water compared to C_3H_7CN could be due to the combination of two factors. First, it could be due to the H-bonding of solvent molecules to the lone pair electrons of the thiocyanato sulfur, as previously noted for cyano complexes of Ru and other related systems.[17] In this case, the energy of the first MLCT transition in different solvents can also be related to the metal-based ruthenium(II/III) oxidation potential. Second, the interaction of the dielectric constant of the solvent with the change in dipole in the excited state of the dye is known to show solvatochromism.[18] It is interesting to note that the variation in energy/peak position of the MLCT bands of complex **3** in different solvents is significantly larger when compared to that of the $\pi-\pi^*$ bands.

2. Emission Studies. Complex **2** has an emission maximum at 813 nm, with an excited-state lifetime of 30 ns. The short excited-state lifetime of complex **2** could be due to the presence of protons on carboxyl groups, enhancing the nonradiative deactivation channel.[19] The emission quantum yield of complex **2** is 0.0004. On the other hand, complexes **3** and **4** show a more intense luminescence at 770 and 800 nm, respectively. The red shift of the low-energy absorption and emission maximum of complex **2** compared to those of **3** and **4** is due to the lower π^* orbital of the 2,2′-bipyridyl-4,4′-dicarboxylic ligand in the protonated form. These assignments are further corroborated by the electrochemical studies in section 4. The solvent dependence of the emission maximum of complex **3** has been gathered in Table 2.

3. Determination of pK_a Values. The pK_a values of complex **2** were determined by UV−vis and emission measurements over the pH range 1−11. A stock solution (5×10^{-5} M) was prepared in 100 cm^3 of 5:1 H_2O/ethanol mixture containing 0.1 M $NaNO_3$. Since the neutral complex **2** was insoluble in water, 20% ethanol was added to avoid the precipitation. The initial pH of the solution was adjusted to 11 by adding 0.2 M NaOH solution. The pH of the solution was lowered by the addition of HNO_3 solution. The acid was added in such a way that throughout the entire measurements the total volume of added acid was negligible. The UV−vis spectrum of each solution was obtained after adding acid and allowing the solution to equilibrate for 5 min. The emission spectra were measured at room temperature by exciting into the lowest-energy MLCT band (550 nm).

Complex **2** at pH 11 shows visible MLCT bands at 500 and 370 nm, and the high-energy $\pi-\pi^*$ band at 308 nm. The ground-state pK_a values can be determined from the relationship between the change in the optical density or the peak maximum with the pH for a given wavelength.[20] When acid is added to an alkaline solution of complex **2**, changes in the electronic spectrum occur as shown in Figure 1a. Upon lowering the pH from 11 to 1, the MLCT transition band shifts from 500 to 520 nm with three clean isosbestic points at 515, 406, and 380 nm.

(12) Zakeeruddin, S. M.; Nazeeruddin, Md. K.; Humphry-Baker, R.; Grätzel, M. *Inorg. Chim. Acta*, in press.
(13) Root, M. J.; Sullivan, B. P.; Mayer, T. J.; Deutsch, E. *Inorg. Chem.* **1985**, *24*, 2731.
(14) Herber, R. H.; Nan, G.; Potenza, J. A.; Schugar, H. J.; Bino, A. *Inorg. Chem.* **1989**, *28*, 938.
(15) Nazeeruddin, Md. K.; Muller, E.; Humphry-Baker, R.; Vlachopoulos, N.; Grätzel, M. *J. Chem. Soc., Dalton Trans.* **1997**, 4571.
(16) Cargill Thompson, A. M: W.; Smailes, M. C. C.; Jeffery, J. C.; Ward, M. D. *J. Chem. Soc., Dalton Trans.* **1997**, 737.
(17) Chen, P.; Meyer, T. J. *Chem. Rev.* **1998**, *98*, 1439.
(18) Curtis, J. C.; Sullivan, B. P.; Meyer, T. J. *Inorg. Chem.* **1983**, *22*, 224. 16.
(19) Nazeeruddin, Md. K.; Kalyanasundaram, K. *Inorg. Chem.* **1989**, *28*, 4251.
(20) Giordano, P. J.; R.Bock, C. R.; Wrighton, M. S.; Interrante, L. V.; Williams, R. F. X. *J. Am. Chem. Soc.* **1977**, *99*, 3187.

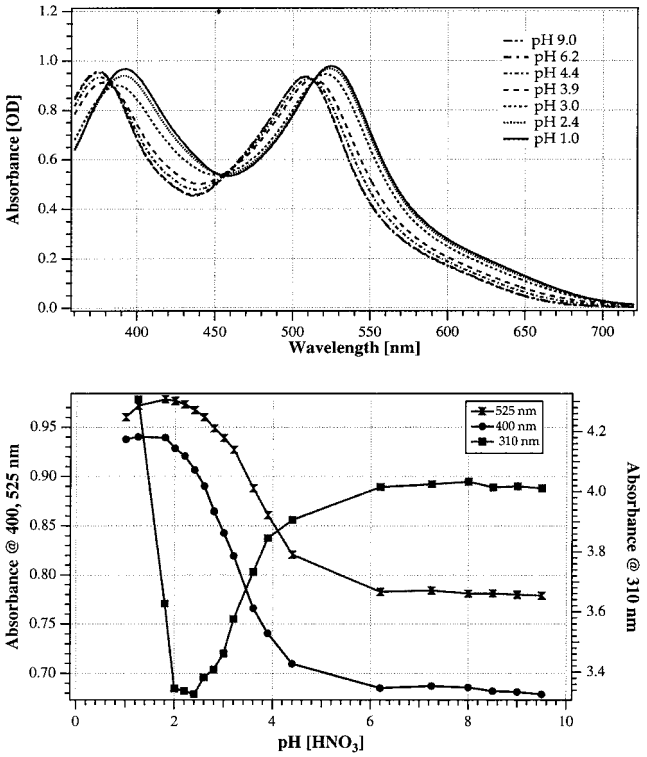

Figure 1. (a, top) Absorption spectral changes of complex **2** as a function of pH at pH 1, 2.4, 3, 3.9, 4.4, 6.2, and 9.0. (b, bottom). Absorbance change as a function of pH in complex **2** at 310, 400, and 525 nm.

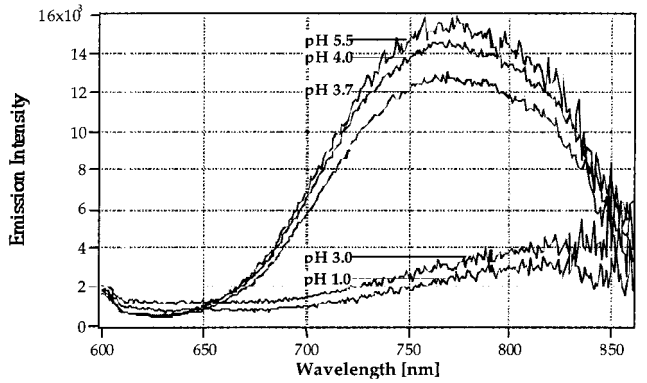

Figure 2. Emission spectral changes of complex **2** as a function of pH between 1 and 5.5. For clarity purposes, spectral data at higher pH are not shown.

The intraligand transition shifts from 308 to 312 nm with an isosbestic point at 305 nm. Figure 1b shows the comparable titration curve, obtained by plotting the λ(max) (MLCT) change at 525, 400, and 310 nm vs pH for complex **2**. The plot shows the expected sigmoidal shape, with the pH at the inflection point giving the ground-state pK_a value of 3 ± 0.1 and another at pH 1.5 ± 0.1. These values are assigned to the pK_{a1} and pK_{a2} of the dcbpy ligand.[19] Back-titration of the same solution quantitatively regenerated the original spectrum.

In complex **2** there are two 4,4′-dicarboxy-2,2′-bipyridine ligands which could give four separate acid−base equilibria, if the dissociation is stepwise. On the other hand, if the dissociation were simultaneous, one would expect one equilibrium constant. The fact that we observe two separate equilibria in complex **2** suggests that the pyridyl subunits are nonequivalent. Scheme 1 presents the simplified two-step equilibrium of complex **2**. Complex **2** shows an emission maximum at 770 nm in alkaline

Scheme 1

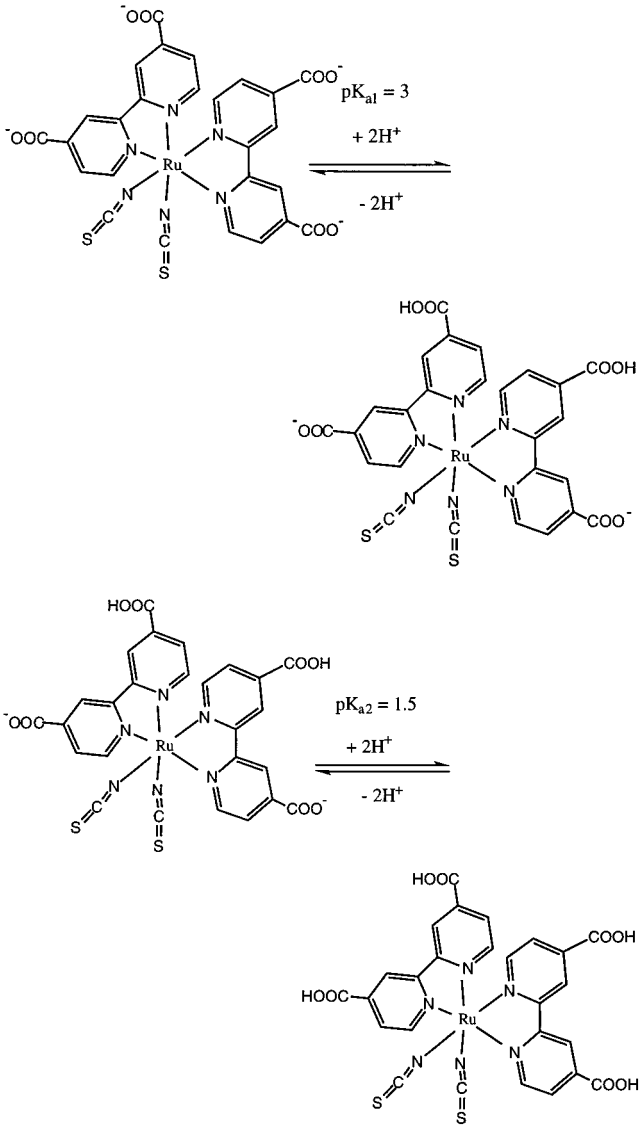

pH, which red shifts to 814 nm upon lowering the pH to 1. Figure 2 shows the change in the emission intensity and maximum with pH. The emission intensity and lifetime decrease with decreasing pH.[21]

4. Electrochemistry. The cyclic voltammetry of complex **3** in acetonitrile shows a reversible wave at 0.57 V vs SCE, which can be readily assigned to the Ru(II)/(III) couple (Figure 3). The oxidation wave is 2 times higher than the reduction wave, suggesting that the complex is not quantitatively regenerated on the time scale of the cyclic voltammogram. On the cathodic side, there is a reversible peak at −1.67 V vs SCE, assigned to the reduction of the dcbpy ligand.

The Ru(II)/(III) couple in complex **3** is shifted ca. 290 mV negatively with regard to that of complex **2**[3c,4,22] due to the replacement of H^+ by tetrabutylammonium cation. The negative shift for the dcbpy-based reduction potential is even larger, i.e., about 600 mV compared to that of complex **2**. This is ascribed to the combination of two factors, i.e., the increase in the LUMO

(21) Lay, P. A.; Sasse, W. H. S. *Inorg. Chem.* **1984**, *23*, 4123. (b) Shimidzu, T.; Iyoda, T.; Izaki, K. *J. Phys. Chem.* **1985**, *89*, 642. (c) Foreman, T. K. Ph.D. Dissertation, University of North Carolina, Chapel Hill, NC, 1982.

(22) Bond, A. M.; Deacon, G. B.; Howitt, J.; MacFarlane, D. R.; Spiccia, L.; Wolfbauer, G. *J. Electroanal. Chem.* **1999**, *146*, 648.

Table 3. ^{1}H NMR Data in the Aromatic Region for the Ruthenium Complexes and the Ligand 4,4′-COOH-2,2-bipyridine in D_2O Solution Containing 0.05 M NaOD[a]

complex/ligand	6	6′	5	5′	3	3′
dcbpy	8.78 (d)		7.87 (dd)		8.40 (d)	
$[Ru(dcbpyH_2)_2(Cl)_2]$	9.84 (d)	7.80 (d)	8.13 (dd)	7.39 (dd)	8.86 (d)	8.69 (d)
$[Ru(dcbpyH_2)_2(NCS)_2]$	9.55 (d)	7.82 (d)	8.22 (dd)	7.52 (dd)	8.94 (d)	8.77 (d)
$[(Bu_4N)_4[Ru(dcbpy)_2(NCS)_2]$	9.50 (d)	7.79 (d)	8.23 (dd)	7.55 (dd)	8.95 (d)	8.78 (d)
$(Bu_4N)_2[Ru(dcbpyH)_2(NCS)_2]$	9.52 (d)	7.80 (d)	8.19 (dd)	7.49 (dd)	8.92 (d)	8.75 (d)
$[Ru(dcbpyH_2)_2(H_2O)_2]$	9.38 (d)	7.78 (d)	8.18 (dd)	7.50 (dd)	8.90 (d)	8.74 (d)

[a] In parts per million with respect to TMS.

Table 4. Crystal Data for $(Ru(dcbbpy)_2(NCS)_2 \cdot 5Os(CH_3)_2)$[a]

fw	1096.28	α (deg)	75.238(2)
cryst color, habit	dark red, thin plate	β (deg)	89.611(2)
cryst dimens (mm)	$0.26 \times 0.10 \times 0.02$	γ (deg)	66.446(2)
cryst syst	triclinic	V (Å^3)	2408.7(2)
space group	$P\bar{1}$	Z	2
a (Å)	11.4663(4)	density(calcd) (g cm^{-3})	1.511
b (Å)	12.5897(5)	T (K)	243(2)
c (Å)	18.9329(7)	no. of obsd reflns, $F6(F)$, used in refinement	4045
		no. of refined params	493
		residuals R, R_w	0.0809, 0.0950

[a] For a full description of structure **2** see ref 11.

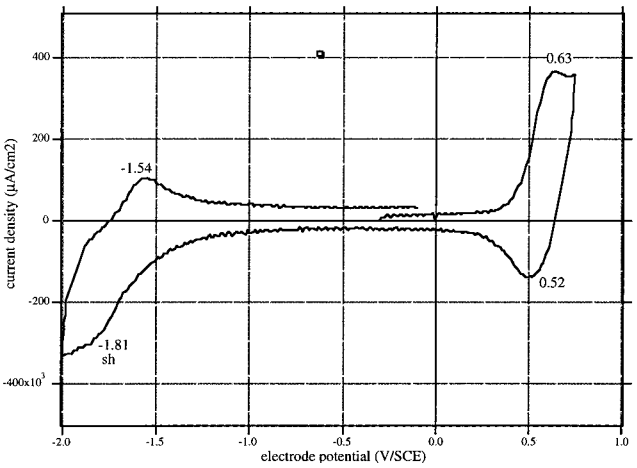

Figure 3. Cyclic voltammogram of complex **3** in CH_3CN at room temperature under argon. The solution concentration is 1.4×10^{-3} M, with 0.1 M TBATFB electrolyte. The working electrode is a Pt microdisk of 25 μm diameter, and the scan rate is 50 V/s.

energy of the ligand caused by the deprotonation and electrostatic effects.

5. NMR Spectroscopy. Complex **1** in a D_2O + NaOD solution shows six peaks in the aromatic region corresponding to two different dcbpy ring protons (Table 3). However, within a few minutes new resonances appear more upfield than those of the dichloro species. We attribute these new peaks to the formation of a new complex due to the substitution of chloride by aqua ligand. Evidence for the substitution of chloride ligand by water can be readily obtained by measuring the NMR spectrum of an authentic *cis*-diaquobis(2,2′-bipyridine-4,4′-$(COO^-)_2$)ruthenium(II) complex in D_2O containing 0.01 M NaOD. After 18 h the chloride substitution by water was more than 90% complete. The NMR spectrum after 18 h shows mainly six resonance peaks at higher field than that of complex **1**. It is striking to note the 0.46 ppm difference in the H-6 proton chemical shift between complex **1** and diaqua species that could result from higher formal charge at the ruthenium center.

Proton NMR spectral data of **2**, **3**, and **4** are collected in Table 3. The resonances in the aromatic region are due to two different dcbpy ring protons, in which two pyridine rings are trans to

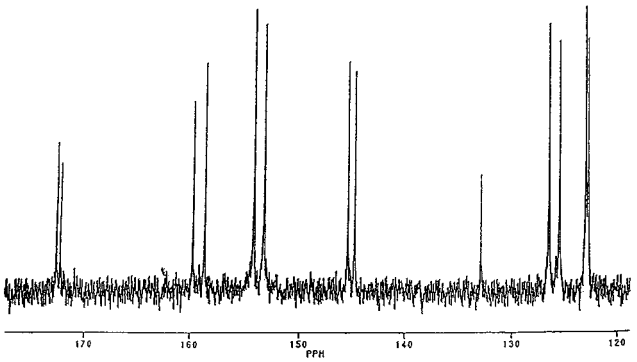

Figure 4. ^{13}C NMR specrum of the $(Bu_4N)_2[Ru(dcbpyH)_2(NCS)_2]$ complex in D_2O + NaOD (0.1 M) at room temperature.

the NCS ligands and the remaining two are trans to each other. We assign the downfield-shifted proton resonances to pyridine rings trans to each other, and the high-field proton resonances to pyridine rings trans to the NCS ligand.[23] The resonance peaks in the aliphatic region for complexes **3** and **4** are due to tetrabutylammonium cations. The integrated ratio of the aliphatic to aromatic protons shows the presence of four and two tetrabutylammonium cations in complexes **3** and **4**, respectively.

The proton-decoupled carbon-13 NMR spectrum of complex **4** in the aromatic region is shown in Figure 4. The different carbon resonances in complex **4** were identified by comparison with known bipyridine complexes.[24] The carbon-13 data are particularly useful in complexes **2**−**4** for determining whether the NCS ligand has N- or S-bonded coordination. It has been reported that S coordination of the NCS ligand to transition metals shields the carbon atom much more than N coordination. S-coordinated NCS ligands show carbon resonances at 120−125 ppm.[8]

The ^{13}C NMR spectrum of complex **4** shows 12 resonance peaks (Figure 4) corresponding to two different pyridine rings and one single peak at 132.84 ppm that we assign to the carbon

(23) Shklover, V.; Nazeeruddin, M.-K.; Zakeeruddin, S. M.; Barbe, C.; Kay, A.; Haibach, T.; Steurer, W.; Hermann, R.; Nissen, H.-U.; Grätzel, M. *Chem. Mater*. **1997**, *9*, 430.
(24) Cook, M. J.; Lewis, A. P.; McAuliffe, G. S. G. *Org. Magn. Reson.* **1984**, *22*, 388.

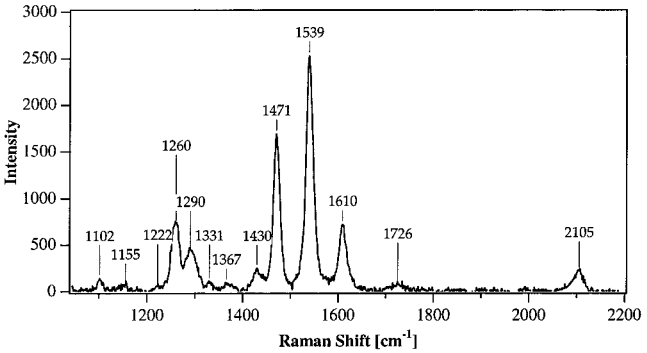

Figure 5. Resonance Raman spectra of the $(Bu_4N)_2[Ru(dcbpyH)_2(NCS)_2]$ complex adsorbed on the TiO_2 surface.

of N-coordinated NCS. The downfield two resonances at 172.59 and 172.24 are assigned to the carboxylate carbons. There is a negative (∼1 ppm) chelation induced shift (CIS, compared to the free ligand) for the C-4 carbons because of dπ donation from the metal center to the ligand. However, C-2 and C-6 carbons show a significant CIS value, ∼4 ppm, because of the σ bonding formation from the lone pair of electrons on the nitrogen to the empty metal orbitals. The CIS values at C-5 and C-3 are smaller, 1 and 2 ppm, respectively. The two peaks at 159.7 and 158.6 are assigned to C-2 and C-2′ carbons, which are near the electron-withdrawing nitrogen of coordinated pyridine. The remaining carbons were assigned on the basis of proton NMR data, and our assignments are consistent with the literature.[24] Aliphatic carbons of tetrabutylammonium cations were observed at 54, 35, 16, and 9 ppm.

6. IR and Resonance Raman Spectra. The NCS^- group has two characteristic modes, ν(NC) and ν(CS), which are frequently considered as diagnostic with respect to the coordination mode of the ambidentate NCS ligand.[25] The IR spectrum of complex **4** shows an intense absorbance at 2120 ν(NC) and 780 ν(CS) cm^{-1} due to the N-coordinated NCS ligand. The two sets of bands at 1720 and 1680 ± 2 cm^{-1} in complex **4** are due to the presence of protonated and deprotonated carboxyl groups. Complex **4** was adsorbed onto the TiO_2 surface, and laser excitation in the MLCT band of complex **4** yields detailed resonance Raman spectra above 1000 cm^{-1}, with bands characteristic of the coordinated polypyridyl vibrations. Figure 5 shows the Raman spectrum of complex **4** obtained by excitation at 415.44 nm (Krypton laser as excitation source) which gave vibrational modes due to the 4,4′-dicarboxy-2,2′-bipyridine ligand at 1610, 1539, 1471, 1290, 1260, and 1102 ± 2 cm^{-1}. The broad and weak vibrational mode at 2105 ± 2 cm^{-1} is due to the coordinated NCS ligand. The intensity of this band is enhanced significantly compared to that of the solution spectrum. The band at 1726 is due to the carbonyl group of the ligand and is a strong indication of an ester-type linkage onto the TiO_2 surface.

7. HPLC of Complexes 2, 3, and 4. Identification of trace amounts of impurities and/or isomers by spectroscopic techniques is a difficult task. Therefore, HPLC was applied to separate the impurities prior to spectroscopic analysis. Application of a diode array detector allows the on-line measurement of the absorption spectra. Wang et al. has successfully used this technique to separate the N2 and N4 isomers of triazole complexes of ruthenium.[26]

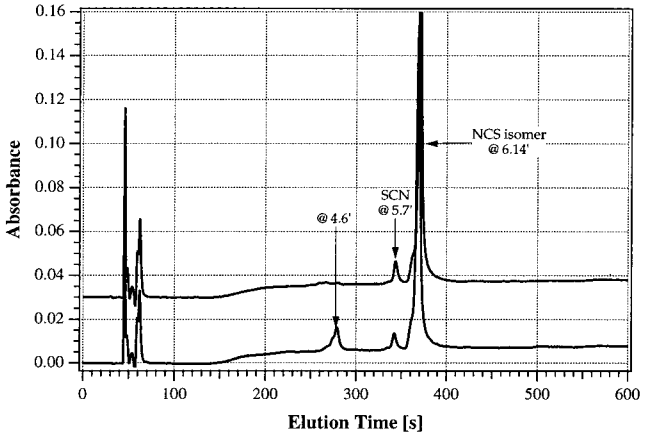

Figure 6. HPLC Chromatogram of the complexes $[Ru(dcbpyH_2)_2(NCS)_2$ (bottom) and $(Bu_4N)_2[Ru(dcbpyH)_2(NCS)_2]$ (top).

Complexes **2**−**4** were analyzed using reversed-phase chromatography that utilized adsorbent silica gel with a modified surface. The eluent is a polar one, acetonitrile/water mixture. The less polar a compound, the longer is the residence time on the stationary phase and therefore the retention time. A higher content of organic solvent in the eluent decreases the interaction and the retention time. To cover a wide spectrum of polarity, an increasing acetonitrile gradient was applied. A small amount of acid was added to the eluent to displace the dissociation equilibrium of the carboxylate groups to the protonated form.

Figure 6, bottom trace, shows the chromatogram of complex **2**, at a detection wavelength of 220 nm. The highest peak at 6.14 min belongs to the desired compound **2**. Besides this main peak, there are two minor peaks, one at 5.7 min and another at 4.6 min. Interestingly, the UV−vis spectra of peaks at 4.6 and 5.7 min are almost identical with that of the peak at 6.14 min. The fact that the absorption spectra are so close, coupled with the small difference in the retention time, is suggestive of the linkage isomers of the thiocyanate ligand.

Figure 6, top trace, shows the HPLC chromatogram of complex **4**, where the retention time is the same as that of complex **2**. The same retention time could be due to the fast exchange of tetrabutylammonium cations by the protons that are present in the mobile phase. The spectrum corresponding to the other small peak at 5.7 min is very similar to that of the main peak. The chromatographic peaks at about 1 min stem from the solvent front. It is interesting to note the presence of only one minor peak at 5.7 min in complex **4**, whereas in complex **2** there are two minor peaks. This shows that, in the process of converting complex **2** to complex **4**, one of the isomers was removed.

We have collected the main peak by using a semipreparative column, and when we reinjected the HPLC-purified sample solution, the chromatogram showed one single peak at the same retention time as the main peak for complex **2**. Therefore, we exclude any possibilities of aggregation or decomposition during chromatography giving rise to additional small peaks. This shows that by transforming **2** into its tetrabutylammonium salts, we are effectively removing at least one linkage isomer. On the basis of the HPLC data, the minor peaks in complexes **2** and **4** are assigned to the linkage isomers of the NCS ligand. However, isolation of the thiocyanate isomer proved difficult because of the low yield of the reaction.

The HPLC analysis of the rhenium complex containing a thiocyanate ligand was reported with the thiocyanate isomer

(25) Wajda, S.; Rachlewicz, K. *Inorg. Chim. Acta* **1978**, *31*, 35.
(26) Wang, R.; Vos, J. G.; Schmehl, R. H.; Hage, R. *J. Am. Chem. Soc.* **1992**, *114*, 1964.

Table 5. Comparison of Bond Lengths and Bond Angles of M−NCS in Complexes with Ru−NCS Moieties

	$[RuL_2(NCS)_2]^a$	$[RuL_2(NCS)_2]^b$	$[RuL_2(NCS)_2]^c$
Ru−NCS	2.05(1)	2.07(1)	2.052(6), 2.059(5)
Ru-bpy_{cis}	2.02(1)	2.04(1)	2.025(5), 2.039(5)
Ru-bpy_{trans}	2.05(1)	2.01(1)	2.055(5), 2.059(5)
N(NCS)−Ru−N(NCS)′	88.7(5)	86(1)	91.3(2)
$N(bpy)_{trans}RuN(bpy)_{cis}$[d]	79.5(5)	78.3(7)	79.1(2), 79.3(2)
$N(bpy)_{trans}RuN(bpy)_{trans}$	90.6(5)	95(1)	91.9(2)
$N(bpy)_{cis}RuN(bpy)_{cis}$	174.5(6)	172(1)	175.0(2)

[a] L = 4,4′-COOH-2,2-bipyridine. [b] L = 4,4′-$COOC_2H_5$-2,2-bipyridine, ref 23. [c] L = 2,2-bipyridine, ref 14. [d] $N(bpy)_{cis}$ and $N(bpy)_{trans}$ refer to the bpy ligands cis and trans to the NCS ligands.

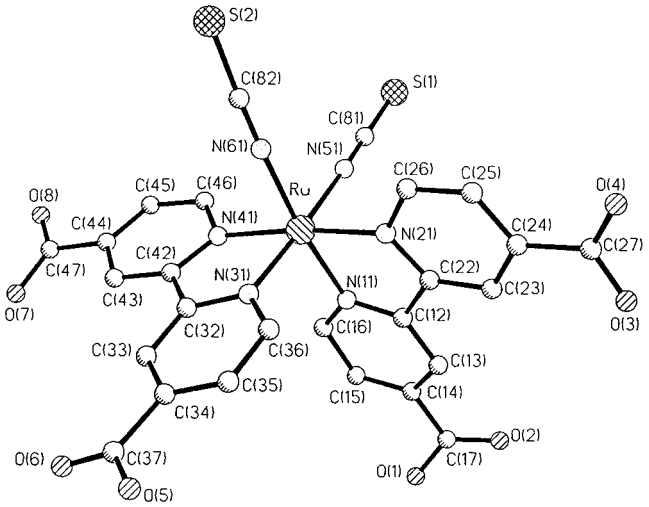

Figure 7. Molecular structure of the complex $[Ru(dcbpyH_2)_2(NCS)_2$.

eluting shortly before the isothiocyanate isomer.[27] Our HPLC data of complex **2** are consistent with the observation for the Re complexes, with the thiocyanate isomer eluting shortly before the isothiocyanate isomer.

8. Crystal Structure and Surface Coordination of Complex 2. Figure 7 shows a perspective view of the complex **2** structure. The molecular structure of **2** shows that the ruthenium adopts a distorted octahedral geometry.[11] The carboxylate groups do not hold the shaded conformation; one of them, viz., C(17)O(1)O(2), is skewed up to 30° from the ideal orientation, which is coplanar with the corresponding aryl moiety. The high temperature factors of the oxygen atoms also indicate certain mobility for these groups. Despite a poor accuracy of the structure and indeterminate positions of H atoms, strong H bonds with solvate DMSO molecules are clearly seen from C(O)O···O(DMSO) distances of 2.47−2.61 Å. These interactions however have little effect on COO rotational oscillations, possibly for much freedom of DMSO molecules, atoms of which have even higher temperature factors, too.

For comparison purposes bond lengths and angles for different crystals of bpy and substituted bpy complexes are gathered in Table 5. The Ru−N (NCS) bond length does not differ significantly for different bipyridine ligands. However, when compared to cobalt complexes, the Ru−NCS bond distance is significantly longer than the Co−NCS bond distance.[28] The variation in the bond distance between the metal and the nitrogen of pyridine ligands is even less (Table 5). The NCS moiety remains approximately linear, 178.7°. Because of the constraints of the dcbpy ligand, the angles N−Ru−N deviate from the idealized values of 90° and 180°. The C_2 symmetry of complex **2** about the bisector line of N(11)Ru(1)N(31) and N(51)Ru(1)N(61) bond angles should be noted. In a projection along this axis the molecule as a two-dimensional object has an inversion center (Ru atom). It is fascinating to note the significant difference between the NCS−Ru−NCS bond angles in complexes containing 2,2′-bipyridine and 4,4′-carboxy-2,2′-bipyridine. In these complexes, as the π acceptor strength decreases, the bond angle approaches the more idealized value of 91°.

The intramolecular distances in **2**, viz., O(1)···O(6) and O(2)···O(5) (Figure 7) are 10.0 Å. The crystal lattice shows that there is no hydrogen bonding among the carboxyl groups and no extended interactions involving the carboxyl groups and NCS ligand. Molecular dynamics calculations have been used to model the interaction of complex **2** with the (101) surface plane of anatase.[11] The most likely configuration supported by recent IR analysis [29] is shown in Figure 8. The dye is attached via two of its four carboxylate groups. The carboxylate either bridges two adjacent rows of titanium ions through bidentate coordination or interacts with surface hydroxyl groups through hydrogen bonds. Of the two remaining carboxylate groups, one is ionized while the other remains in the protonated state.

9. Photovoltaic Performance. The performance of **2**, **3**, or **4** as a sensitizer on a nanocrystalline TiO_2 electrode has been studied. The photocurrent action spectra obtained with the TiO_2 films coated with a monolayer of these complexes are shown in Figure 9. The preparation of the nanostructured TiO_2 films and experimental details for the measurements were given earlier.[30] The dye solutions were prepared in 1:1 v/v acetonitrile and *tert*-butyl alcohol solvent mixture at a concentration of 5×10^{-4} M. The TiO_2 electrodes were heated at 450 °C for 20 min under an O_2 atmosphere and cooled to 100 °C before being dipped into the dye solution. The electrodes were left in the solution for 12−15 h. The redox electrolyte consisted of a solution of 0.6 mol of dimethylpropylimidazolium iodide and 50 mmol of I_2 in methoxyacetonitrile.

The incident monochromatic photon-to-current conversion efficiency (IPCE) is plotted as a function of excitation wavelength. The photocurrent action spectra of these sensitizers show broad features covering a large part of the visible spectrum (Figure 9). The IPCE value in the plateau region is 80% for complex **2** while for complex **3** it is only about 66%. In the red region, the difference is even more pronounced. Thus, at 700 nm the IPCE value is twice as high for the fully protonated complex **2** as compared to the deprotonated complex **3**. As a consequence the short-circuit photocurrent is 17.5−18.5 mA/cm^2 for complex **2**, while it is only about 12−13 mA/cm^2 for complex **3**. However, there is a tradeoff inasmuch as the

(27) Jurisson, S.; Halihan, M. M.; Lydon, J. D.; Barnes, C. L.; Nowotnik, D. P.; Nunn, A. D. *Inorg. Chem.* **1998**, *37*, 1922.
(28) Buckingham, D. A.; Clark, C. R.; Liddell, G. F.; Simpson, *J. Aust. J. Chem.* **1993**, *46*, 503.
(29) Finnie, K. S.; Bartlett, J. R.; Woolfrey, J. L. J. *Langmuir* **1998**, *14*, 2744.
(30) Zakeeruddin, S. M.; Nazeeruddin, Md. K.; Humphry-Baker, R.; Grätzel, M.; Shklover, V. *Inorg. Chem.* **1998**, *37*, 5251.

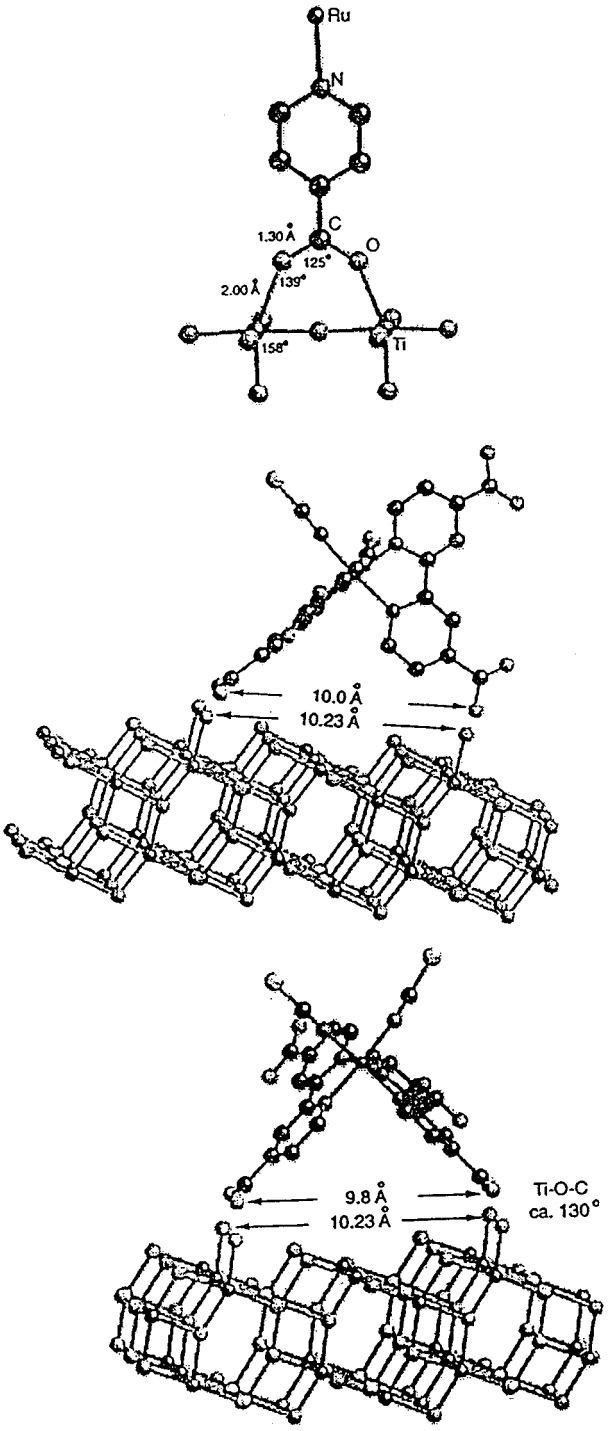

Figure 8. Surface binding of the $[Ru(dcbpyH_2)_2(NCS)_2$ complex on the (101) surface of anatase.

photovoltage is about 200 mV higher for the latter as compared to the former sensitizer. Nevertheless, this is insufficient to compensate for the current loss. Hence, the photovoltaic performance of complex **4** carrying two protons is superior to that of compounds **2** and **3** that contains four and no protons, respectively. The doubly protonated form of the complex is therefore preferred over the other two sensitizers for sensitization of nanocrystalline TiO_2 films.

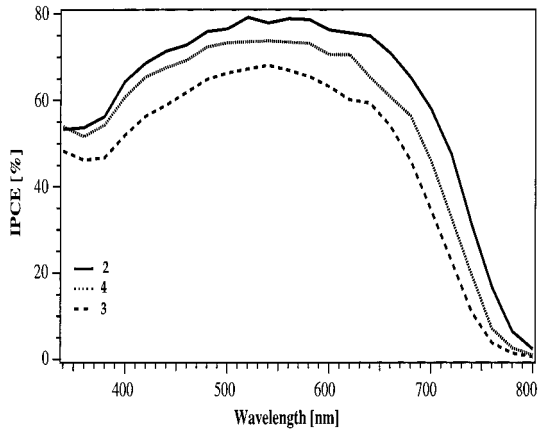

Figure 9. Photocurrent action spectra of nanocrystalline TiO_2 films sensitized by complexes **2**, **3**, and **4**. The incident photon to current conversion efficiency is plotted as a function of wavelength.

Conclusions

We made a quantitative analysis of the absorption and emission spectral changes of complex **2** with pH and solvent. In the ground state, the dissociation of protons was sequential ($pK_a = 3$ and 1.5). The Ru(II)/(III) couple in complex **3** is shifted ca. 290 mV negatively with regard to that of complex **2** due to the replacement of H^+ by tetrabutylammonium cation. The negative shift for the dcbpy-based reduction potential is even larger, i.e., about 600 mV compared to that of complex **2**. Carbon-13 NMR provides a convenient means to obtain the mode of NCS coordination to the metal center. IR and crystal structure data unambiguously establish that the N-bonded isothiocyanate is the thermodynamically more stable isomer. The molecular crystal structure of $[Ru(dcbpyH_2)_2(NCS)_2]$ and its possible anchoring modes on the TiO_2 surface were examined. HPLC data show possible linkage isomers of complex **2**. The performances of these complexes as photosensitizers in the nanocrystalline TiO_2-based solar cell were investigated. We have shown the important effect exerted by the proton content of the complex on both the short-circuit photocurrent and open-circuit photovoltage of dye-sensitized nanocrystalline solar cells. The doubly protonated form of the dye exhibited power conversion efficiency superior to those of the other two sensitizers.

Acknowledgment. We are grateful to the Swiss Energy Office and INAP for financial support. We also acknowledge Drs. K. Kalyanasundaram, P. Péchy, and F. P. Rotzinger for their helpful discussions and Ms. U. Michalczik and P. Comte for their excellent help with the laboratory work.

IC990916A